PERGAMON

Journal of Structural Geology 22 (2000) 401–409

JOURNAL OF STRUCTURAL GEOLOGY

www.elsevier.nl/locate/jstrugeo

Feasibility of estimating cementation rates in a brittle fault zone using Sr/Ca partition coefficients for sedimentary diagenesis

Jafar Hadizadeh[a,*], Franklin F. Foit[b]

[a]*Department of Geography and Geosciences, University of Louisville, Louisville, KY 40292, USA*
[b]*Department of Geology, Washington State University, Pullman, WA 90168, USA*

Received 5 March 1999; accepted 29 October 1999

Abstract

Cement phases such as calcite or quartz often incorporate trace elements from the parent fluids as they crystallize. Experimental sedimentary diagenesis indicates that trace element partition coefficients reflect rates of cementation. The applicability of these findings to fault zone cementation is examined as we make a preliminary attempt to estimate calcite cementation rate in a brittle fault zone directly from the fault-rock composition data. Samples for this study were collected from the Knoxville outcrop of the Saltville fault in Tennessee. The cementation rates for the fault rock samples range from 1×10^{-12} to 3×10^{-13} m^3/h per m, in agreement with some experimental rates and the rates reported for samples from the DSDP sites. When applied to a non-responsive pore-system model, these rates result in rapid precipitation sealing indicating the influence exerted by the surface-area/volume ratio of the pore network. We find it feasible to obtain a reasonable range of values for the cementation rate using the trace element partition method. However, the study also indicates the need for relatively accurate values for the trace/carrier element ratio in the fault zone syntectonic pore fluid, and exhumed cement.

1. Introduction

Models of syntectonic fluid flow indicate extensive involvement of fluids in faulting with a diverse range of salinities (Fyfe et al., 1978; Kerrich, 1986; Oliver, 1986; McCaig, 1988; Wannamaker, 1994). Furthermore, studies of exhumed fault zones support models in which fluid flow in brittle faults occurs cyclically in tune with seismic activity of the faults (Fisher and Brantley, 1992; Sibson, 1992; Logan and Decker, 1994). According to the fault valve model (Sibson, 1992) coseismic deformation in a brittle fault zone generates a net volume of new connective porosity and a fluid-pressure gradient that results in rapid mixing of fault zone fluids, with fluids flowing in from the surrounding rocks. Enhanced pore connectivity has been reported for cases of failure by faulting as well as deformation by cataclastic flow in a variety of lithologies (Zoback and Byerlee, 1975; Zhang et al., 1994; Peach and Spiers, 1996). Following a seismic event, precipitation sealing could occur under hydrothermal conditions primarily by mineral solubility changes in response to changes in pressure and species concentration, and fresh reaction surface area offered by highly comminuted materials. Modeling and experimental studies suggest that the precipitation followed by compaction creep has the potential to hydraulically seal off large sections of the interior of a fault (Blanpied et al., 1992; Byerlee, 1993; Sleep and Blanpied, 1994; Scholz et al., 1995). The resulting fluid-pressure build-up provides a basis for models of the seismic cycle in general and an explanation for the phenomenon of weak faults in particular. A key question, therefore, is the rate at which common siliceous and carbonate cements precipitate under brittle fault zone conditions.

* Corresponding author.
E-mail address: hadizadeh@louisville.edu (J. Hadizadeh).

0191-8141/00/$ - see front matter
PII: S0191-8141(99)00172-8

Syntectonic brittle fault zones and diagenetic environments evolve under similar *P–T*-hydrologic regimes in the shallow crust. Numerous studies have been dedicated to processes of precipitation sealing, compaction, low-temperature recrystallization, and pressure solution, which are common in both environments (Maxwell, 1960; Baker et al., 1980; Groshong, 1988; Hajash and Bloom, 1991; Hickman and Evans, 1991; Robin, 1992; Newman and Mitra, 1994; Canals and Meunier, 1995; Scholz et al., 1995; Lemee and Gueguen, 1996; Hacker, 1997; Karner et al., 1997; Olsen et al., 1998). Experimental diagenesis has resulted in a wealth of knowledge, particularly on the kinetics of carbonate cementation. It is well known from studies in sedimentary diagenesis that the composition of cement minerals and their primary trace elements hold useful information on fluid composition and rates of precipitation (see reviews by McIntire, 1963; Mucci and Morse, 1990). This paper is a preliminary attempt to apply some of the findings of experimental diagenesis to the question of syntectonic precipitation sealing rates in brittle faults.

1.1. Some precepts from sedimentary diagenesis

In a sedimentary system, cement phases such as calcite or quartz often incorporate trace elements from the parent fluids, mostly through surface reactions, as they crystallize (McIntire, 1963; Mucci and Morse, 1990). At equilibrium, the ratio of trace element ions in the fluid to those being embedded in the solid phase should remain constant. The ratio, known as the trace element partition coefficient, reflects pressure and temperature, degree of saturation of the precipitating species, and reaction rates (Morse and Bender, 1990). The partition coefficient in a solution reservoir large enough to buffer the concentration changes during precipitation is usually quantified by the non-thermodynamic Henderson–Kracek distribution law,

$$(C_t/C_C)_{solid} = D_t(C_t/C_C)_{solution} \quad (1)$$

where D is the homogeneous partition coefficient, C_t and C_C are the molar concentrations of the trace and carrier ions, respectively. The Doerner–Hoskins logarithmic partition law,

$$\ln(C_{It}/C_{Lt}) = \lambda(C_{Ic}/C_{Lc}) \quad (2)$$

where λ is the partition coefficient, C_I and C_L denote the initial and final solution concentrations of the trace and carrier species, is applicable where the parent solution is not buffered and the products tend to be compositionally zoned. In the case of calcite, the value of the trace element partition coefficient increases with increasing rate of precipitation in a systematic manner (Kinsman and Holland, 1969; Lorens, 1981; Mucci, 1986; Pingitore and Eastman, 1986; Morse and Bender, 1990; Beck et al., 1992).

Commonly, the relationship between precipitation rate (R), saturation state (Ω), and rate constant (k) is expressed by the empirical kinetic equation:

$$R = k(\Omega - 1)^n \quad (3)$$

or its logarithmic form:

$$\log R = \log k + n \log(\Omega - 1) \quad (4)$$

where n constitutes the reaction order (Morse, 1983; Mucci and Morse, 1986; Lee and Morse, 1999). Mucci (1986) precipitated magnesian calcites at room temperature from a solution with the composition and ionic strength of seawater and at $\Omega_{calcite}$ values ranging from 2.0 to 14.4. The results, combined with those of Mucci and Morse (1983) (approximately 45 precipitation experiments) were used to obtain the empirical relationship:

$$D_{Sr} = 0.0622 \log R + 0.539 \quad (5)$$

where R is the precipitation rate in mol/h per m^2, D_{Sr} is the Sr/Ca partition coefficient as defined in Eq. (1). We note that the exact nature of this rate-dependence is not clear, Eq. (5) is the result of a least square fit with a correlation coefficient of 0.62. In addition, the extent of the effect of Mg as an inhibitor ion, and partial pressure of CO_2 (P_{CO_2}), on the precipitation rate of calcite has not been ascertained. Beck et al. (1992), in agreement with the results of Mucci and Morse (1983, 1990) and Jacobson and Usdowski (1976), reported no significant effect on D_{Sr} value due to increase in pressure. These workers observed only a slight increase in D_{Sr} value with increasing temperature in experiments carried out to 400°C and 500 bars of pressure. A similar expression was obtained for λ_{Sr} by Lorens (1981) who used Doerner–Hoskins heterogeneous distribution law to evaluate the Sr/Ca partition coefficient.

2. Fault rock composition data

Samples for this study were collected from the Sharp Gap outcrop of the Saltville thrust in the city of Knoxville, Tennessee, in the southern Appalachians in the United States. The fault outcrop, described in detail by Hadizadeh (1994), consists of a 1.5- to 2-m-wide damage zone enclosing a 15–20-cm-wide core of highly comminuted, but fully cohesive rocks. The main shear zone and its immediate wallrocks sampled for this study occur within the Lower Ordovician Mascot dolostone (Harris, 1971; Churnet et al., 1982). The core region of the fault consists mostly of very fine-grained cataclasites and ultracataclasites. Rocks outside of the fault core are crush breccias, microbreccias,

protocataclasites and coarse-grained cataclasites. There is microstructural evidence for pervasive pressure solution deformation in the cataclastic rocks at the Sharp Gap outcrop. A persistent cm-scale banding fabric associated with the cataclastic rocks appears to be due to bundles of millimeters to micron-scale, dark-colored seams intermittent with very fine-grained cataclasites and ultracataclasites. Microprobe and XRD analyses of the bands indicated the presence of clay minerals and probably microcrystalline to amorphous quartz (Hadizadeh, 1994). The fault-rock classification proposed by Sibson (1977) was used to differentiate the cm- and mm-scale internal structures of the fault zone in hand specimens and petrographic slides. Samples for compositional analyses were obtained from these structural units by scraping or microdrilling. Analytical work was carried out by X-ray fluorescence spectrometry (XRF) using an automated Rigaku 3370 spectrometer. Major, minor, and trace element compositions were analyzed on 2:1 $Li_2B_4O_7$ flux/rock-powder fused beads. The results were normalized on a volatile-free basis. The effects of loss on ignition (LOI) and Fe_2O_3 content on accuracy was checked by comparing our results with British Chemical Standard 368 dolomite and the National Bureau of Standards 1-C argillaceous limestone for which LOI and oxidation-state data were available.

The analyses showed that CaO, MgO, SiO_2, K_2O, Na_2O made up to 99% or more of the host and the fault rock sample compositions. Petrographic analyses show that calcite forms the cataclastic cement in these rocks (Hadizadeh, 1994). Given the petrographic composition data, a simplified tri-modal (dolomite, calcite and quartz/clay) composition model was adopted. The oxide-to-modal calculations were carried out following

Table 1
Modal and trace element composition profile of the fault rocks derived from the XRF data[a]

Sample	Rock	Dol.%	Qtz./clay	$CaCO_3$%	Sr ppm
U4	Host	64.53	35.47	0.00	111
U5i	Host	66.55	33.45	0.00	107
U6	Host	59.48	40.52	0.00	97
H13iv	cb	50.46	30.28	19.25	189
H13ii	fcb	63.57	21.74	14.68	201
H13i	fcb	45.78	11.51	42.71	313
H1i	pc	16.90	62.84	20.26	173
H14i	uc	0.00	20.04	79.96	508
C3	pc	13.70	41.20	45.10	226
C4a	uc	11.00	20.10	68.90	345
Cg	c	16.56	43.84	39.61	205
C7	c	13.17	42.11	44.73	223
C8	uc	9.07	59.21	31.72	143
F4ii	pc	2.65	56.93	20.42	132
F11vii	pc	39.72	48.00	12.28	172
F11iii	fcb	17.87	58.17	23.97	184
F3i	pc	16.56	43.84	39.61	127
F2ii	pc	13.17	42.11	44.73	158
U7	Host	88.03	11.74	0.23	132
U9	Host	84.90	11.04	4.06	156

[a] U = undeformed; C = core; H = hanging wall damage zone; F = footwall damage zone; fcb = fine crush breccia; cb = crush breccia; pc = protocataclasite; c = cataclasite; uc = ultracataclasite. Analytical accuracy ($\pm 1\sigma$): $SiO_2 = \pm 0.30\%$, $Al_2O_3 = \pm 0.08\%$, FeO = ±0.27%, CaO = ±0.05%, MgO = ±0.01%, $K_2O = \pm 0.01\%$, Sr = ±1.49 ppm. Combined instrumental and bead preparation precision ($\pm 1\sigma$): $SiO_2 = \pm 0.06\%$, $Al_2O_3 = \pm 0.04\%$, FeO = ±0.09%, CaO = ±0.03%, MgO = ±0.02%, $K_2O = \pm 0.01\%$, Sr = ±1.43 ppm.

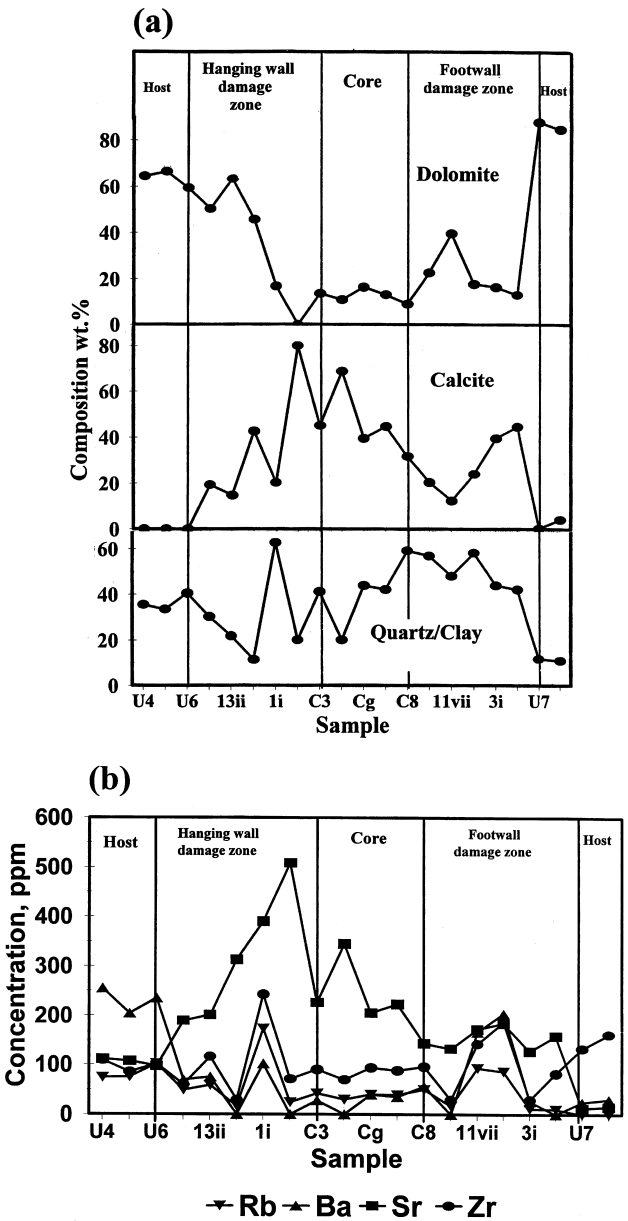

Fig. 1. The Saltville fault composition profiles (see Table 1 for data). (a) Simplified modal composition profile. (b) Trace element profiles. The host is dolostones and dolomitic shales of the Mid-Ordovician Knox Group. Note the strong correlation between Sr and the calcite cement in the samples.

a procedure described by Hadizadeh (1994). The modal and trace element composition for samples are presented in Table 1, where the actual spatial order of sampling is maintained. The profile plot of the modal composition and the significant trace elements (Fig. 1) indicate that Sr is the chief trace element associated with the calcite cement in the fault rocks. The asymmetric form of the Sr profile with respect to the fault core probably reflects the asymmetry of fluid activity in the fault zone.

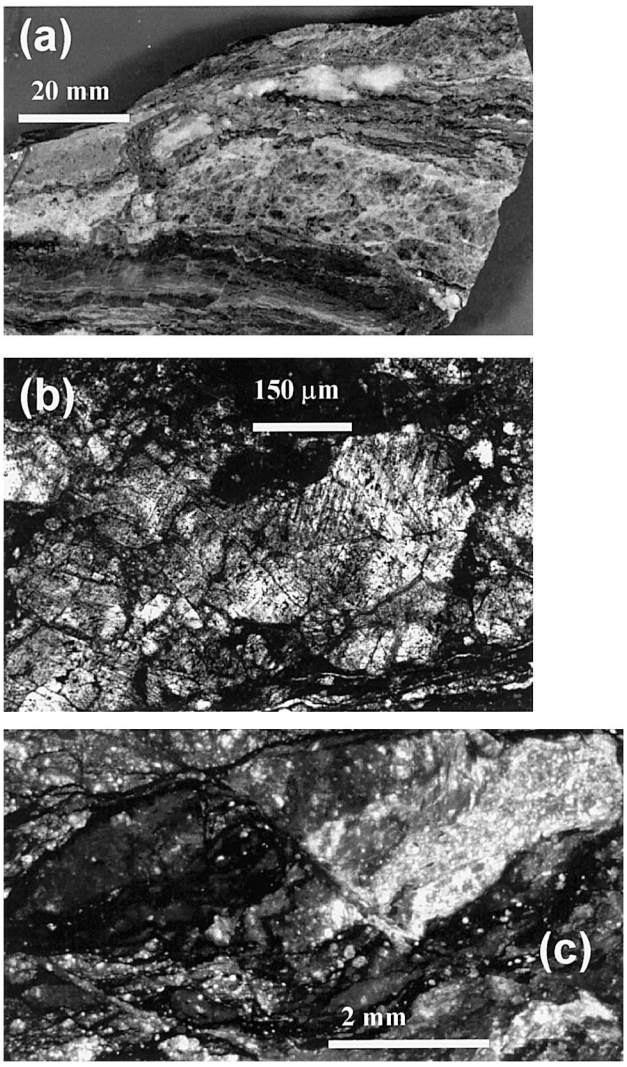

Fig. 2. Typical Saltville fault cataclastic microstructures, which indicate that the calcite cement is syntectonic (crossed polars). (a) A lens of well-cemented crush breccias in sample F11iii. Note micro-faulted calcite veins below the lens. (b) Microfractures and twinning in calcite clasts from the cement in sample C7. (c) A micro-breccia clast with internal cataclastic banding similar to the fine bands in (a) above. Sample C8.

3. Timing of the cement in cataclastic rocks

The compositional analyses of the pervasive syntectonic cement mineral in a suite of cataclastic rocks should provide concentration values to be used in the $(C_t/C_C)_{solid}$ term in Eq. (1). To what extent is the bulk of the cementing mineral syntectonic? An essential step is to examine the cement for evidence of deformation and reworking. In the Saltville fault zone, an abundance of microstructural deformation in the calcite cement and evidence of extensive pressure solution deformation led to the conclusion that the intergranular cement was mainly derived from the host-rock dolomites through interaction of pressure solution and cataclasis (Hadizadeh, 1994). Three types of microstructural evidence are used to support the notion that the cataclastic cement in the Saltville fault rocks is syntectonic. First, the cement-bearing bands of cataclasites are often separated by anastomosing pressure solution seams (Fig. 2a). The cataclasites are lens-shaped at the outcrop scale and have sharp boundaries. We do not find a cross-cutting vein network in the core region which might have fed the cataclasite lenses after their formation. Secondly, the calcite cement in the cataclasite and ultracataclasite lenses shows definite signs of grain-scale deformation in the form of twinning (Fig. 2b). Thirdly, the presence of breccia-sized clasts, with an internal cataclastic banding and its own 'intergranular' calcite cement from earlier episodes of cataclasis (Fig. 2c) suggest that the cement was involved in deformation throughout the development of the fault rocks.

At a preliminary level, therefore, we assume that calcite cement in the fault rocks is entirely syntectonic and we proceed to calculate Sr/Ca ratios for our samples. For this purpose the cement's actual trace el-

Table 2
The Sr/Ca ratio for the Saltville fault calcite cement[a]

Sample	Rock	Ca%	Sr ppm	mSr/mCa × 10^{-4}
H13iv	cb	7.7	106	6.29
H13ii	fcb	5.9	96	7.50
H13i	fcb	17.1	238	6.36
H1i	pc	8.1	145	8.19
H14i	uc	32.0	508	7.26
C3	pc	18.1	203	5.15
C4a	uc	27.6	327	5.42
Cg	c	15.8	178	5.13
C7	c	17.9	201	5.14
C8	uc	12.7	128	4.61
F4ii	pc	8.2	95	5.30
F11vii	pc	4.9	107	9.92
F11iii	fcb	9.6	155	7.37
F3i	pc	15.8	100	2.88
F2ii	pc	17.9	136	3.48

[a] See Table 1 for rock and sample abbreviations.

Table 3
Ionic strength[a] vs depth, and Sr/Ca ion ratios in some continental waters

Depth	I	mSr^{2+}/mCa^{2+}	Comments and reference
0–50 m	0.01	NA	carbonate aquifer, central Pennsylvania, USA (Langmuir, 1971)
40–70	0.045	9.86×10^{-3}	mine waters and boreholes, SE France (Aquilina et al., 1997)
240	0.02	7.03×10^{-3}	saline and thermal groundwater, Cornwall, England (Edmunds et al., 1985)
300	0.13	6.90×10^{-3}	saline and thermal groundwater, Cornwall, England (Edmunds et al., 1985)
327	0.21	NA	interstitial waters, SE France (Aquilina et al., 1997)
634	0.265	9.75×10^{-3}	scientific borehole, SE France (Aquilina et al., 1997)
690	0.40	7.40×10^{-3}	saline and thermal groundwater, Cornwall, England (Edmunds et al., 1985)
300–600	0.505	1.38×10^{-2}	saline groundwater, central Missouri, USA (Banner et al., 1989)
908–969	0.017	4.34×10^{-3}	water from Stripa Granite, Stripa, Sweden (Nordstrom et al., 1989)
1829–2115	0.023	8.67×10^{-3}	water from Cajon pass drillhole, California, USA (Kharaka et al., 1988)
1–4 km?	0.513	1.60×10^{-2}	fault-related spring waters, Rumsey Hills, California, USA (Davison, 1995)
Seawater	0.66	1.00×10^{-2}	average value (Fyfe et al., 1978)

[a] Ionic strength $I = 1/2 \sum m_i Z_i^2$, where m_i and Z_i are the ith ions concentration and charge, respectively, was calculated for sample Ca^{2+}, Mg^{2+}, Na^+, K^+, Cl^-, HCO_3^- and SO_4^{2+} molar concentrations.

ement concentrations should be used. The XRF analyses of our samples, however, provide Sr concentration values which include Sr from both the cement and clasts. To determine an Sr concentration value for each sample's cement we can write $Sr_{cement} = Sr_{sample} - Sr_{clast}$. The strontium content of the clasts could be estimated as follows. Since Sr_{clast} originates in the host dolomites (Sr_{host}), the amount of Sr in clasts varies in proportion to a ratio of dolomite in the sample (S_{dol}), to the dolomite in the host rock, (H_{dol}), or:

$$Sr_{clast} = [S_{dol}/H_{dol}]Sr_{host}. \quad (6)$$

Mean values of 0.727 ppm for H_{dol} and 120.6 ppm for Sr_{host} from Table 1 were used to arrive at the values given for the cement in Table 2. It should be noted that although this feasibility study uses the mass–balance relationship [Eq. (6)] to acquire the cement's Sr values, it is important to find more accurate values for $(C_t/C_C)_{solid}$ by analyzing the cataclastic cement separately for its Sr content. A number of analytical methods might be recommended for this purpose. The cement Sr values could be obtained by electron microprobe, or estimated from EDS (Energy Dispersive Spectrometer) elemental maps of representative samples. Alternatively, it is possible to obtain Sr concentration values directly by applying ICP (Inductively Coupled Plasma), or XRF (X-ray fluorescence) analysis to micro drilled samples of the cataclastic cement.

4. Fault zone syntectonic pore fluid

Estimating D_{Sr} for the fault zone precipitation reactions via Eq. (1) requires that a value for the ratio of trace-element to carrier-element in the syntectonic fault zone pore fluid be determined [i.e. the term $(C_t/C_C)_{solution}$]. The diagenetic calcite precipitation models including those behind the empirically derived Eqs. (1)–(5) often use seawater or seawater analogs. Since this study did not include a fluid inclusion analysis, and none were available for the Saltville fault rocks, the question of applicability of these equations in a case involving continental fault pore-fluids prompted us to compare the chemistry of the fluids from these environments in order to evaluate the possible errors involved. The data summarized in Table 3 and shown in Fig. 3 suggest that in general, continental pore waters may be comparable to seawater in terms of ionic strength and composition at depths greater than 0.5 km. A greater degree of leaching by slow-moving pore-water at elevated temperatures and mixing with formation fluids account for the differences between the chemistry and salinity of shallow aquifer waters and the deeper-level pore waters. Fluid inclusion studies of exhumed fault rocks (Parry, 1994) reveal that some fault zone fluids contain as much as 20 equivalent weight percent of NaCl concentration. It is notable

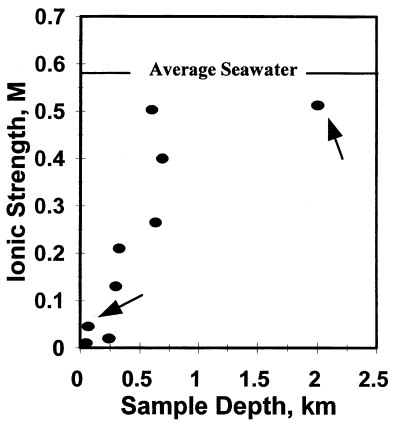

Fig. 3. Ionic strength of some continental pore waters. Arrows indicate the upper and lower values selected to represent the fault zone syntectonic pore fluid. See Table 3 for data sources.

Table 4
Range of calcite precipitation rates for the fault damage zone

	$(m\mathrm{Sr}/m\mathrm{Ca})_{solid}$	D_{Sr}	R_{high}, m^3/h per m^{2a}	D_{Sr}	R_{low}, m^3/h per m^{2a}
Hdz[b] mean	7.12×10^{-4}	0.072	1.15×10^{-12}	0.051	5.28×10^{-13}
Fdz[b] mean	5.79×10^{-4}	0.058	7.08×10^{-13}	0.042	3.77×10^{-13}

[a] Using 10^{-3}(mol calcite/h per m^2 × gfw)/$\rho_{calcite}$ to convert calcite precipitation rates from mol/h per m^2 to m^3/h per m^2.
[b] Hdz and Fdz are the hanging wall and footwall damage zones, respectively.

that NaCl provides most of the ionic strength for diagenetic reactions in the case of marine deposits. Davisson et al. (1994) argued that fault-related spring waters expelled from depths of up to 4 km in Rumsey Hills, California, may actually represent modified seawater. Nevertheless, the data in Table 3 also indicate that the seawater diagenesis models may not be directly applicable to fault zones. On the basis of data in Table 3 alone, the continental waters differ from each other and from seawater in Sr^{2+}/Ca^{2+} values by a factor of about three, noting that this may not be viewed as a maximum possible error. It is, therefore, instructive to either carry out fluid inclusions analysis to establish the salinity of the fault's syntectonic pore fluid, or direct studies at fault outcrops where the fault pore fluid composition has already been characterized.

5. Precipitation rate estimates for the Saltville fault

The $m\mathrm{Sr}^{2+}/m\mathrm{Ca}^{2+}$ values of 1.38×10^{-2} and 9.86×10^{-3} from Table 3 were selected to represent the high and low values, respectively, for (C_{Sr}/C_{Ca}) in the syntectonic pore fluid of the fault zone. Table 4 lists the molar (Sr/Ca) mean values for the damage zone cement, the calculated D_{Sr} using Eq. (1), and the calcite precipitation rates (R) using Eq. (5). A number of workers have studied the effect of temperature on precipitation rate of calcite in sedimentary environments. Beck et al. (1992) found an approximately linear increase in R from 2.65×10^{-10} to 2.11×10^{-8} m^3/h per m^2 with increasing temperature from 250 to 400°C. In contrast, Lorens (1981), Busenberg and Plummer (1986), Shiraki and Brantley (1995) and Deleuze and Brantley (1997) reported values of 1.05×10^{-10} m^3/h per m^2 at 25°C to 8.77×10^{-6} m^3/h per m^2 at 100°C. Analysis of the Sr/Ca ratio in sediments from DSDP sites by Baker et al. (1982) suggested calcite precipitation rates in the order of 1.2×10^{-16} (500 m depth, 22°C) to 4.4×10^{-18} m^3/h per m^2 (seafloor) which seem to be in good agreement with the results of Beck et al. (1992). While these results may not be used to draw a quantitative rate–temperature relationship, they suggest that calcite precipitation rate is temperature-dependent. Assuming that brittle deformation in our samples occurred between 100 and 250°C, the estimated damage zone precipitation rates of 1.15×10^{-12} to 3.77×10^{-13} m^3/h per m^2 (see Table 4) appear to be in agreement with the experimental results of Beck et al. (1992) and the rates based on samples from the DSDP sites by Baker et al. (1982). However, compared to some other experimental results (Deleuze and Brantley, 1997), precipitation rates for the damage-zone appear to be at least an order of magnitude slower.

5.1. Implications for precipitation sealing

Formation sealing and pressure seals due to cementation are more extensively researched and better understood in sedimentary environments than in fault zones. Model studies indicate that post-seismic precipitation in the fault zones need not clog all the newly generated porosity in order to seal the fault core (Sleep and Blanpied, 1994). This is reasonable because the creation of coseismic porosity is constrained by energy requirements of work against elevated confining pressures (Marone et al., 1990; Sleep and Blanpied, 1992) which favors connective microcracks and microfractures with large surface-area to volume ratios.

Episodic precipitation in the Saltville fault damage zone would have occurred due to a reduction in the solubility of $CaCO_3$ in the supersaturated $CaCO_3$–$MgCO_3$ system with lowered Mg ion concentration (Hadizadeh, 1994). The precipitation rate estimates for the fault (Table 4) can be translated into sealing times using a rock material, with appropriate pore-distri-

Table 5
Precipitation sealing times for a non-responsive model of the damage zone

P_{ai}, m^2/g	P_d, μm	P_{vi}, m^3/g	$\%P_{vf}$,[a] %	t_{low}, year	t_{high}, year
1.0×10^{-6}	123.29	7.00×10^{-12}	0.23	6358	2084
1.0×10^{-5}	48.78	1.34×10^{-12}	0.47	1217	399
8.9×10^{-5}	18.04	5.00×10^{-10}	1.75	510	167
0.0002	10.11	7.00×10^{-10}	2.46	318	104
0.0003	3.32	3.00×10^{-10}	1.05	91	30
0.0001	1.73	5.00×10^{-10}	1.75	45	15
0.0425	0.36	1.10×10^{-8}	38.60	23.5	7.7
0.101	0.18	6.70×10^{-9}	23.51	6.03	1.98
0.318	0.04	7.40×10^{-9}	25.96	2.12	0.69
0.277	0.02	1.20×10^{-9}	4.21	0.39	0.13

[a] P_{vf} is the pore volume fraction.

bution properties, as a non-responsive model, or a template. In trials with a variety of sandstone and limestone, the per unit mass pore-distribution properties of the Indiana limestone (350 μm grain size, 6.5% porosity) appeared to be a suitable template for the seismic porosity of the damage zone rocks for the reasons described in the following. Mercury porisometer data presented in Table 5 for the limestone were collected using a Micromeritic Pore-Sizer 9300 mercury porisometer (LeRavalec et al., 1996) in the 0.1–200 MPa pressure range. A high proportion of microcracks porosity in the seismic porosity of the damage zone is represented by the template's size–volume distribution, where more than 90% of the total pore volume is due to pores in the 0.02–2.0 μm size-range. The same population of pores is also responsible for over 99% of the pore surface area with potential for immediate post-seismic fluid–rock interactions. It should be noted that only the pore-distribution properties and not the lithology of the template is of significance here.

For the purpose of this discussion, the portion of total seismic porosity that affects short-term permeability of the fault zone will be called transient porosity (Δ). We then define sealing time (t) as the time required to eliminate the transient porosity by precipitation of a solid phase, or basically $t = \Delta/R$. We also assume that Δ is about 30% of the co-seismically generated porosity (total porosity in the template). This cutoff value is largely speculative for the lack of data, but is mainly based on data from Scholz et al. (1995) which noted a pore pressure increase from 50 MPa to 65 MPa for about a 30% decrease in porosity due to precipitation in their hydrothermal sealing experiments. The sealing times for the two average values of R (Table 4) were calculated using the relationship:

$$t = 0.3P_{vi}/(R \times P_{ai}) \quad (7)$$

where P_{vi} and P_{ai} are the incremental pore volume and surface area, respectively. Plots of the model damage zone sealing time vs. pore volume fraction and pore diameter are shown in Fig. 4. A precipitation sealing would occur in less than 10 years for $P_d \leq 2$ μm (~94% of the transient pore volume), and in less than 1 year in pores which have crack-like dimensions ($P_d \leq 0.2$ μm). It is evident that the relatively slow cementation rates for the fault zone have produced rather short sealing times because of high surface-area to volume ratio of the model pore-system. The slower sealing-time range of 100–1000 years for the volumetrically insignificant population of pores in the transient fraction supports the notion of a less interrupted background fluid flow (leakage) between fault zone and the host at time scales that exceed the return time of major seismic events in tectonically active regions. It should be noted that the pore-system model we used does not represent fracture openings, which may be common in the rock mass at larger scales and particularly at shallower depths. Consequently, this may be taken to imply that rapid sealing is generally confined to below certain depths where limitations on the volume of seismic porosity preclude fluid flow via larger conduits. However, it has been argued that the short-term permeability of fault rocks at any confining pressure is primarily controlled by connectivity through microcracks (Bruhn, 1994; Parry et al., 1991).

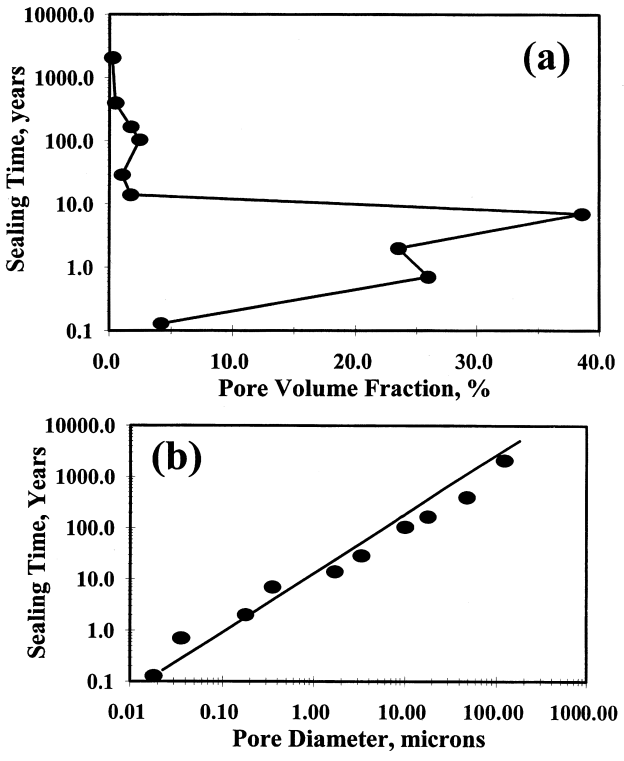

Fig. 4. Precipitation sealing time for a non-responsive model of the fault damage zone. (a) Sealing time vs. pore volume fraction. (b) Log–linear relationship between sealing time and pore diameter.

6. Conclusions

1. It has been possible to obtain a reasonable range of estimates for the rate of calcite precipitation in the Saltville fault damage zone by applying Sr/Ca partition coefficients, derived from precipitation experiments in sedimentary diagenesis, to composition data from the fault zone.
2. The fault damage-zone calcite precipitation rates are in agreement with some experimental sedimentary rates obtained in the 22 to 400°C temperature range, but appear to be slow compared to results obtained by others in experiments conducted between 25 and 100°C. Applied to a model pore sys-

tem representing coseismic porosity with large surface area to volume ratio, the resulting fault zone precipitation sealing rates yield short sealing times.
3. Several important assumptions had to be made regarding the timing of the cement in the samples and composition of the syntectonic fault zone fluids, most of which could be eliminated, or made more accurate by additional analytical work. Ultimately, however, experimental modeling of cementation under fault zone conditions and analyses of actual fault zone fluids would have to provide constraints on precipitation rates in that environment.

Acknowledgements

The authors wish to thank Diane Johnson from Washington State University analytical laboratory. We highly appreciate reviews by James P. Evans, William T. Parry and Peter Vrolijk. Acknowledgement is made to donors of the Petroleum Research Fund, administered by the American Chemical Society (J.H.), for support of this research through the grant ACS-PRF#22907-B2.

References

Aquilina, L., Sureau, J.F., Steinberg, M., 1997. Comparison of surface, aquifer- and pore-waters from a Mesozoic basin and its underlying Paleozoic basement, southeast France: Chemical evolution of waters and relationship between aquifers. Chemical Geology 138, 185–209.

Baker, P.A., Kastner, M., Byerlee, D.A., 1980. Pressure solution and hydrothermal recrystallization of carbonate sediments: an experimental study. Marine Geology 38, 185–203.

Baker, P.A., Gieskes, J.M., Elderfield, H., 1982. Diagenesis of carbonates in deep-sea sediments—Evidence from Sr/Ca ratios and interstitial dissolved SR2+ data. Journal of Sedimentary Petrology 52, 71–82.

Banner, J.L., Wasserburg, G.J., Dobson, P.F., Carpenter, A.B., Moore, C.L., 1989. Isotopic and trace element constraints on the origin and evolution of saline groundwaters from central Missouri. Geochimica et Cosmochimica Acta 53, 383–398.

Beck, J.W., Berndt, M.E., Seyfried, W.E., 1992. Application of isotope doping techniques to evaluation of reaction kinetics and fluid/mineral distribution coefficients: An experimental study of calcite at elevated temperatures and pressures. Chemical Geology 97, 125–144.

Blanpied, M.L., Lockner, A.M., Byerlee, J.D., 1992. An earthquake mechanism based on rapid sealing of faults. Nature 358, 574–576.

Bruhn, R.L., 1994. Fracturing in normal fault zones: Implications for fluid transport and fault stability. In: Hickman, S., Sibson, R.H., Bruhn, R. (Eds.), Proceeding Workshop LXIII, The Mechanical Involvement of Fluids in Faulting, Volume Open File Report 94-228. U.S. Geological Survey, pp. 231–246.

Busenberg, E., Plummer, L.M., 1986. A comparative study of the dissolution and crystal growth kinetics of calcite and aragonite. U.S. Geological Survey Bulletin 1578, 139–168.

Byerlee, J.D., 1993. Model for episodic flow of high-pressure water in fault zones before earthquakes. Geology 21, 303–306.

Canals, M., Meunier, J.D., 1995. A model for porosity reduction in quartzite reservoirs by quartz cementation. Geochimica et Cosmochimica Acta 59, 699–709.

Churnet, H.G., Misro, K.C., Walker, K.R., 1982. Deposition and dolomitization of Upper Knox carbonate sediments, Copper Ridge district, east Tennessee. Geological Society of America Bulletin 93, 76–96.

Davison, I., 1995. Fault slip evolution determined from crack–seal veins in pull-aparts and their implications for general slip models. Journal of Structural Geology 17, 1025–1034.

Davisson, M.L., Presser, T.S., Criss, R.E., 1994. Geochemistry of tectonically expelled fluids from the northern Coast ranges, Rumsey Hills, California, U.S.A. Geochimica et Cosmochimica Acta 58, 1687–1699.

Deleuze, M., Brantley, S.L., 1997. Inhibition of calcite crystal growth by Mg+2 at 100°C and 100 bars: Influence of growth regime. Geochimica et Cosmochimica Acta 61, 1475–1485.

Edmunds, W.M., Kay, R.L.F., McCartney, R.A., 1985. Origin of saline groundwaters in the Carnmenellis granite (Cornwall, England): Natural processes and reaction during hot dry rock reservoir circulation. Chemical Geology 49, 287–301.

Fisher, D.M., Brantley, S.L., 1992. Models of quartz overgrowth and vein formation: deformation and episodic fluid flow in an ancient subduction zone. Journal of Geophysical Research 97, 20043–20061.

Fyfe, W.S., Price, N.J., Thompson, A.B., 1978. Fluids in the Earth's Crust. Elsevier, Amsterdam.

Groshong, R.H., 1988. Low-temperature deformation mechanisms and their interpretations. Geological Society of America Bulletin 100, 1329–1360.

Hacker, B.R., 1997. Diagenesis and fault valve seismicity of crustal faults. Journal of Geophysical Research 102, 24459–24467.

Hadizadeh, J., 1994. Interaction of cataclasis and pressure solution in a low-temperature carbonate shear zone. Pure and Applied Geophysics 143, 255–280.

Hajash, A., Bloom, M.A., 1991. Marine diagenesis of feldspathic sand: A flow-through experimental study at 200°C, 1 kb. Chemical Geology 89, 359–377.

Harris, L.D., 1971. Lower Paleozoic paleoaquifer—The Kingsport Formation and Mascot Dolomite of Tennessee and southwest Virginia. Economic Geology 66, 735–743.

Hickman, S.H., Evans, B., 1991. Growth of grain contacts in halite by solution-transfer. Implications for diagenesis, lithification, strength recovery. In: Hickman, S.H. (Ed.), Fault Mechanics and Strength Recovery. Academic, San Diego, pp. 253–280.

Jacobson, R.L., Usodowski, H.E., 1976. Partitioning of strontium between calcite, dolomite and liquids: An experimental study under higher temperature diagenetic conditions, and a model for the prediction of mineral pairs for geothermometry. Contributions in Mineralogy and Petrology 59, 171–185.

Karner, S.L., Marone, C., Evans, B., 1997. Laboratory study of fault healing and lithification in simulated fault gouge under hydrothermal conditions. Tectonophysics 277, 41–55.

Kerrich, R., 1986. Fluid infiltration into fault zones: Chemical, isotopic, mechanical effects. Pure and Applied Geophysics 124, 225–268.

Kharaka, Y.K., Ambats, G., Evans, W.C., White, A.F., 1988. Geochemistry of water at Cajon Pass, California. Preliminary results. Geophysical Research Letters 15, 1037–1040.

Kinsman, D.J., Holland, H.D., 1969. The co-precipitation of cations with $CaCO_3$ IV. The co-precipitation of Sr^{2+} with aragonite between 16 and 96°C. Geochimica et Cosmochimica Acta 33, 1–17.

Langmuir, D., 1971. The geochemistry of some carbonate ground

waters in central Pennsylvania. Geochimica et Cosmochimica Acta 35, 1023–1046.

Lee, Y.-J., Morse, J.W., 1999. Calcite precipitation in synthetic veins: implications for the time and fluid volume necessary for vein filling. Chemical Geology 156, 151–170.

Lemee, C., Gueguen, Y., 1996. Modeling of porosity loss during compaction and cementation of sandstones. Geology 24, 875–878.

LeRavalec, M., Darot, M., Reuschle, T., Gueguen, Y., 1996. Transport properties and microstructural characteristics of a thermally cracked mylonite. Pure and Applied Geophysics 146, 207–227.

Lorens, R.B., 1981. Sr, Cd, Mn and Ca distribution coefficients in calcite as a function of calcite precipitation rate. Geochimica et Cosmochimica Acta 45, 553–561.

Logan, J.M., Decker, C.L., 1994. In: Hickman, S., Sibson, R., Bruhn, R. (Eds.), Cyclic fluid flow along faults, pp. 190–203.

McCaig, A.M., 1988. Deep fluid circulation in fault zones. Geology 16, 867–870.

McIntire, W.L., 1963. Trace element partition coefficient: A review of theory and application to geology. Geochimica et Cosmochimica Acta 27, 1209–1264.

Marone, C., Raleigh, C.B., Scholz, C.H., 1990. Frictional behavior and constitutive modeling of simulated fault gauge. Journal of Geophysical Research 95, 7007–7026.

Maxwell, J.C., 1960. Experiment on compaction and cementation of sand in rock deformation. Memoir of the Geological Society of America 79, 105–132.

Morse, J.W., 1983. The kinetics of calcium carbonate dissolution and precipitation. In: Reeder, R.J. (Ed.), Carbonates. Mineralogy and Chemistry. Mineralogical Society of America, pp. 227–267.

Morse, J.W., Bender, M.L., 1990. Partition coefficients in calcite. Examination of factors influencing the validity of experimental results and their application to natural systems. Chemical Geology 82, 265–277.

Mucci, A., 1986. Growth kinetics and composition of magnesian calcite overgrowths precipitated from seawater. Quantitative influence of orthophosphate ions. Geochimica et Cosmochimica Acta 50, 2255–2265.

Mucci, A., Morse, J.W., 1983. The incorporation of Mg^{2+} and Sr^{2+} into calcite overgrowths: Influence of growth rate and solution composition. Geochimica et Cosmochimica Acta 47, 217–233.

Mucci, A., Morse, J.W., 1990. Chemistry of low-temperature abiotic calcites: Experimental studies on coprecipitation, stability, fractionation. Aquatic Sciences 3, 217–245.

Newman, J., Mitra, G., 1994. Fluid-influenced deformation and recrystallization of dolomite at low temperatures along a natural fault zone, Mountain City window, Tennessee. Geological Society of America Bulletin 106, 1267–1280.

Nordstrom, D.K., Ball, J.W., Donahoe, R.J., Whittemore, D., 1989. Groundwater chemistry and water–rock interactions at Stripa. Geochimica et Cosmochimica Acta 52, 1727–1740.

Oliver, J., 1986. Fluids expelled tectonically from orogenic belts: their role in hydrocarbon migration and other geologic phenomena. Geology 14, 99–102.

Olsen, M.P., Scholz, C.H., Leger, A., 1998. Healing and sealing of a simulated fault gouge under hydrothermal conditions: Implications for fault healing. Journal of Geophysical Research 103, 7421–7430.

Parry, W.T., 1994. In: Hickman, S., Sibson, R., Bruhn, R. (Eds.), Fault fluid compositions from fluid inclusion observations, pp. 334–348.

Parry, W.T., Hedderly-Smith, D., Bruhn, R.L., 1991. Fluid inclusion and hydrothermal alteration on the Dixie Valley fault, Nevada. Journal of Geophysical Research 96, 19733–19748.

Peach, C.J., Spiers, C.J., 1996. Influence of crystal plastic deformation on dilatancy and permeability development in synthetic salt rock. Tectonophysics 256, 101–128.

Pingitore, N.E., Eastman, M.P., 1986. The coprecipitation of Sr^{2+} with calcite at 25°C and 1 atm. Geochimica et Cosmochimica Acta 50, 2195–2203.

Robin, P.F., 1992. Pressure solution-to-grain contacts. Geochimica et Cosmochimica Acta 42, 1383–1389.

Scholz, H.H., Leger, A., Karner, S.L., 1995. Experimental diagenesis. Exploratory results. Geophysical Research Letters 22, 719–722.

Shiraki, R., Brantley, S.L., 1995. Kinetics of near-equilibrium calcite precipitation at 100°C. An evaluation of elementary reaction-based and affinity-based rate laws. Geochimica et Cosmochimica Acta 59, 1457–1471.

Sibson, R.H., 1977. Fault rocks and fault mechanics. Journal of the Geological Society of London 133, 191–213.

Sibson, R.H., 1992. Implications of fault valve behavior for rupture nucleation and recurrence. Tectonophysics 211, 238–294.

Sleep, N.H., Blanpied, M.C., 1992. Creep, compaction and the weak rheology of major faults. Nature 359, 687–692.

Sleep, N.H., Blanpied, M.L., 1994. Ductile creep and compaction. A mechanism for transiently increasing fluid pressure in mostly sealed fault zones. Pure and Applied Geophysics 143, 9–40.

Wannamaker, P.E., 1994. Fluids in the earth's crust: Electromagnetic influences on existence and distribution. In: Hickman, S., Sibson, R., Bruhn, R. (Eds.), Proceeding Workshop LXIII, The Mechanical Involvement of Fluids in Faulting, Volume Open File Rep. 94-228, U.S. Geological Survey, pp. 162–177.

Zhang, S., Cox, S.F., Paterson, M.S., 1994. The influence of room temperature deformation on porosity and permeability in calcite aggregates. Journal of Geophysical Research 99, 15761–15775.

Zoback, M.D., Byerlee, J.D., 1975. The effect of microcrack dilatancy on the permeability of Westerly granite. Journal of Geophysical Research 80, 752–755.